Emergence of macroscopic directional motion of deformable active cells in confined structures

Bao-quan Ai [1,2,*] Jian Ma,[1] Chun-hua Zeng,[3,†] and Ya-feng He[4,‡]

[1]*Guangdong Provincial Key Laboratory of Quantum Engineering and Quantum Materials,*
School of Physics and Telecommunication Engineering, South China Normal University, Guangzhou 510006, China
[2]*Guangdong-Hong Kong Joint Laboratory of Quantum Matter, South China Normal University, Guangzhou 510006, China*
[3]*Faculty of Science, Kunming University of Science and Technology, Kunming 650500, China*
[4]*College of Physics Science and Technology, Hebei University, Baoding 071002, China*

There is now growing evidence of collective turbulentlike motion of cells in dense tissues. However, how to control and harness this collective motion is an open question. We investigate the transport of deformable active cells in a periodically asymmetric channel by using a phase-field model. We demonstrate that collective turbulent-like motion of cells can power and steer the macroscopic directional motion through the ratchet channel. The active intercellular forces proportional to the deformation of cells can break thermodynamical equilibrium and induce the directional motion. This directional motion is caused by the ratchet effect rather than the spontaneous symmetry breaking. The motion direction is determined by the asymmetry of the channel. Remarkably, there exits an optimal nonequilibrium driving (depending on the active strength, the elasticity, and the packing fraction) at which the average velocity reaches the maximum. In addition, the optimized packing fraction and the optimized minimum width of the channel can facilitate the directional motion of cells. Our findings are relevant to understanding how macroscopic directional motion relates to the local force transmission mediated by cell-cell contacts in cellular monolayers.

I. INTRODUCTION

Collective cell motion in dense tissues plays an important role in vital physiological processes including pithelial mesenchymal transition [1,2], cancer invasion [3], wound healing [4], and tissue morphogenesis [5]. Cells are usually driven far from equilibrium through intrinsic energy injection by their biological constituent elements. The active force from microscopic energy input can lead to the spontaneous emergence of large-scale collective behavior, including phase separation [6], flocking [7], topological defect pair production [8], mesoscale turbulence [9], spontaneous flow transition in active polar gels [10], and turbulent collective flows in epithelial cell monolayers [11]. In a few engineered instances, chaotic active motion can be stabilized into directed flows through geometrical constraints [12–19]: spontaneous shear flow in confined cellular nematics [12], macroscopic directional motion in populations of motile colloids [15], flow states of an active nematic in a three-dimensional channel [14], spontaneous motion in hierarchically assembled active matter [17], and chiral edge current in nematic cell monolayers [19]. These examples suggest the possibility of harnessing chaotic active motion through the special devices.

In previous works, cells in a monolayer are isotropic in shape, and most studies of epithelial cells have neglected shape deformations. Recently, Mueller and coworkers [20,21] presented a phase-field model of cellular monolayer based on cell deformation and found that the local active forces proportional to the deformation of cells can drive the system out of equilibrium. Owing to the nematic nature of the interactions, the total force is approximately zero at the tissue level, and no macroscopic directional motion appears under periodic boundary conditions. In addition, the chaotic motion of active matter can be translated into a self-sustained coherent flow [12–19], but the direction of the coherent flow is random and cannot be controlled. An interesting question is therefore whether the local active force from the deformation of cells can break the thermodynamic equilibrium of the system and lead to the macroscopic directional motion through the specially geometrical constraints. The ratchet model provides a strategy that can rectify the random motion to a given direction [22–37]. The ratchet setup is a means to get directed transport without net forces, which is originally conceived to rectify stochastic motion and describe operational principles of biological motors. The ratchet setup can convert the random motion into the directional motion, which requires two necessary conditions: asymmetry and nonequilibrium driving. Therefore, it is of great interest to explore how active turbulence driven by shape deformation is rectified into macroscopic directional motion.

In this work, we address this question for a dense tissue system consisting of deformable active cells in a ratchet
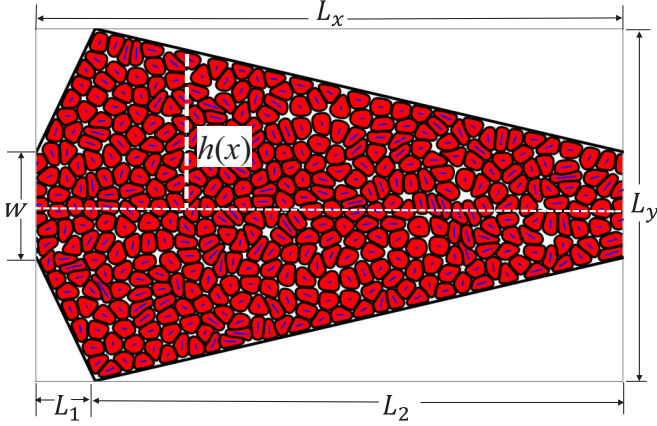
*aibq@scnu.edu.cn
†zchh2009@126.com
‡heyf@hbu.edu.cn

FIG. 1. Schematic of deformable active cells moving in a periodic channel defined by Eq. (1) with the period L_x. The active intercellular forces resulting from force transmission across cell junctions are defined from the nematic tensor in Eq. (8). The active forces here are extensile ($\zeta > 0$), which compresses cells into an elongated form, forcing them to squeeze between neighboring cells. The blue line denotes the long axis of each cell. The shape of the channel described by the half width $h(x)$ described in Eq. (1). The parameter $\Delta = (L_1 - L_2)/L_x$ determines the asymmetry of the channel. W is the minimum width of the channel. A periodic boundary condition is imposed on both ends of the channel and repulsive interaction with the boundary of the channel.

channel. Cells in the channel are modeled as deformable active droplets using a phase-field model. We find that collective turbulent-like motion of cells can be controlled and utilized in a ratchet channel. More specifically, we find the following. First, we find emergence of the macroscopic directional motion induced by the local active forces between cells based on their deformations. The local active forces can break thermodynamical equilibrium and induce the macroscopic directional motion in the ratchet channel. The directional motion is due to the ratchet effect rather than the spontaneous symmetry breaking. The direction of the macroscopic motion is determined by the asymmetry of the channel. Second, we find the optimized directional motion of cells caused by the optimal parameters. There exist optimal parameters (the minimum width of the channel, the packing faction, and the activity strength) at which the average velocity of cells takes its maximal value. Our results are helpful to understand how macroscopic directional motion relates to the microscopic dynamics in cellular monolayers.

II. MODEL AND METHODS

We consider N deformable active cells moving in a two-dimensional periodic channel with the period L_x. Periodic boundary condition imposed in the x direction and hard wall boundaries in the y direction. The shape of the channel as shown in Fig. 1 is described by the half width $h(x)$,

$$h(x) = \begin{cases} \frac{W}{2} + \frac{L_y - W}{2L_1}x, & 0 \leqslant x < L_1, \\ \frac{W}{2} + \frac{L_y - W}{2L_2}(L_x - x), & L_1 \leqslant x < L_x, \end{cases} \quad (1)$$

where L_x and W are the period and the minimum width of the channel, respectively. For convenience, we define $L_x/L_y = 3/2$. The channel is blocked at $W = 0$ and straight at $W = L_y$. The asymmetry of the channel is determined by $\Delta = (L_1 - L_2)/L_x$, and the channel is symmetric at $\Delta = 0$.

In the phase-field model, cells are modeled as deformable active droplets. Unlike in hard-disk and active network models [38], in the phase-field model the membrane of each cell can be continuously deformable. The shape of each cell is defined using an individual phase field, while its velocity is given by a force-balance equation. The phase field of cell i satisfies the equation of motion [20,21,39–43],

$$\partial_t \phi_i + \boldsymbol{v}_i \cdot \boldsymbol{\nabla} \phi_i = -\frac{\mathcal{F}}{\delta \phi_i}, \quad (2)$$

where ϕ_i and $\boldsymbol{v}_i$ are the phase field and the velocity of cell i, respectively. The exterior and interior of cell i corresponds to $\phi_i = 0$ and $\phi_i = 1$, respectively, with a diffusive interface of length λ connecting the two regions and the midpoint, $\phi_i = 1/2$, describing the cell boundary.

The role of the total free energy $\mathcal{F}$ is both to define interactions between cells as well as to maintain the cell integrity. The total free energy [20,21,39,40] is given by $\mathcal{F} = \mathcal{F}_{CH} + \mathcal{F}_{\text{area}} + \mathcal{F}_{\text{rep}} + \mathcal{F}_{\text{wall}}$, where

$$\mathcal{F}_{CH} = \sum_i \frac{\gamma}{\lambda} \int d\mathbf{x} \big[4\phi_i^2(1 - \phi_i)^2 + \lambda^2(\boldsymbol{\nabla}\phi_i)^2\big],$$

$$\mathcal{F}_{\text{area}} = \sum_i \mu \left(1 - \frac{1}{\pi R^2} \int d\mathbf{x}\phi_i^2\right)^2,$$

$$\mathcal{F}_{\text{rep}} = \sum_i \sum_{j \neq i} \frac{k}{\lambda} \int d\mathbf{x}\phi_i^2\phi_j^2,$$

$$\mathcal{F}_{\text{wall}} = \sum_i \frac{k_w}{\lambda} \iint d\mathbf{x}\phi_i^2\phi_w^2. \quad (3)$$

Here $\mathcal{F}_{CH}$ is the Cahn-Hilliard free energy [44] that stabilizes the cell interface and γ the elasticity. The free energy $\mathcal{F}_{\text{area}}$ describes the cell compressibility by imposing a soft constraint with strength μ, restricting the preferred area of each cell to πR^2, where R is the average radius of each cell. This force causes cells to relax to circles in the absence of other forces. The free energy $\mathcal{F}_{\text{rep}}$ accounts for the repulsive cell-cell interactions, which penalizes overlap between cells with an energy scale k/λ. The free energy $\mathcal{F}_w$ defines the repulsive interaction with the boundary of the channel, by placing a fixed phase field along the boundaries defined as $\phi_w = \exp(-2d)$ where d is the distance to the nearest wall and k_w/λ controls the repulsion between the wall ϕ_w and cell ϕ_i.

The velocity $\boldsymbol{v}_i$ for cell i moving on a substrate can be obtained from an overdamped force-balance equation,

$$\xi \boldsymbol{v}_i = \boldsymbol{F}_i^{\text{total}}, \quad (4)$$

where ξ is the friction coefficient between cells and the substrate. $\boldsymbol{F}_i^{\text{total}}$ is the total force acting on the cell i and is calculated as the integral of the local force density weighted by

ϕ_i and a macroscopic tissue stress tensor $\boldsymbol{\sigma}^{\text{tissue}}$ [20,21,39,40]

$$F_i^{\text{total}} = \int d\mathbf{x} \phi_i \nabla \cdot \boldsymbol{\sigma}^{\text{tissue}}; \qquad (5)$$

here $\boldsymbol{\sigma}^{\text{tissue}}$ is usually separated into passive and active stresses [20,21]

$$\boldsymbol{\sigma}^{\text{tissue}} = -P\mathbf{I} - \zeta\mathbf{Q}, \qquad (6)$$

where $\mathbf{Q}$ and P are the tissue nematic tensor and tissue pressure, respectively. ζ is the activity strength, and $\mathbf{I}$ is the unity tensor. The tissue pressure P is obtained from the total free energy $\mathcal{F}$ [20,21,39,40],

$$P = \sum_i \left(\frac{\delta\mathcal{F}_{\text{rep}}}{\delta\phi_i} + \frac{\delta\mathcal{F}_{\text{wall}}}{\delta\phi_i} - \frac{\delta\mathcal{F}_{CH}}{\delta\phi_i} - \frac{\delta\mathcal{F}_{\text{area}}}{\delta\phi_i} \right). \qquad (7)$$

The tissue nematic tensor $\mathbf{Q}$ is defined based on the cell deformation [20,21],

$$\mathbf{Q} = \sum_i \phi_i \mathbf{S}_i, \qquad (8)$$

where $\mathbf{S}_i$ is the deformation tensor [20,21] of cell i given by

$$\mathbf{S}_i = -\int d\mathbf{x} \left\{ (\nabla\phi_i)^T \nabla\phi_i - \frac{1}{2}\text{tr}[(\nabla\phi_i)^T \nabla\phi_i] \right\}, \qquad (9)$$

whose eigenvectors and eigenvalues describe the orientation and strength of the main deformation axes of each cell, respectively. This active force leads to a cell either pushing or pulling on its neighboring cells depending on their position relative to the elongation axis. The system shows an activity-driven transition to nonzero nematic order and flows for large active strength ζ [20]. The deformation of cells is contractile for $\zeta < 0$ and extensile for $\zeta > 0$. Contractile forces make cells circular, and the interactions at the interfaces tend to restore the equilibrium shape, while extensile forces compress cells into an elongate form, giving rise to significant cell-cell rearrangement. In our study, we consider only the extensile case ($\zeta > 0$).

To characterize the coordinated motion of cells, we measure the average velocity of cells. Because directed transport occurs only in the x direction, the average velocity of cells along the x direction in the asymptotic long-time regime can be obtained from the following formula:

$$V_x = \lim_{t \to \infty} \frac{\Delta X(t)}{t}, \qquad (10)$$

where $\Delta X(t) = \frac{1}{N}\sum_{i=1}^N \langle x_i(t) - x_i(0) \rangle$ is the average displacement of cells at time t along the x direction. $x_i(t)$ is the center of mass of cell i. The symbol $\langle \cdots \rangle$ denotes an average over the random initial conditions. To describe the density of particles in the channel, we define the ratio between the area occupied by particles and the total available area as the packing fraction $\varphi = 2N\pi R^2/[L_x(L_y + W)]$. For the high packing fraction φ in excess of 1, cells on average overlap.

Equations (2)–(5) are simulated using a finite difference scheme on a square lattice with a predictor-corrector step. The integration time step was chosen to be 0.005, and the total integration time was more than 4×10^5 (this time is sufficient to ensure that the system can reach a steady state). For all simulation runs, we start with a set of N random cell positions
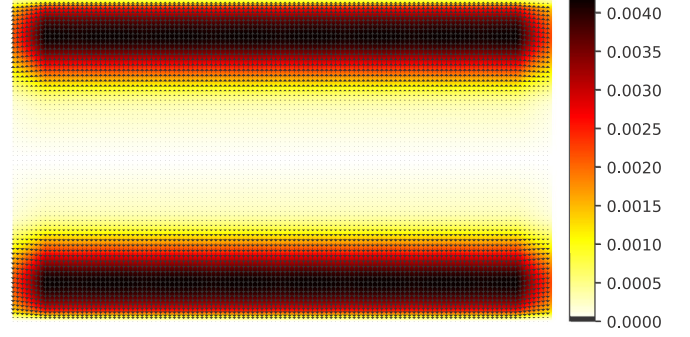
(a) $\zeta = 0.001$
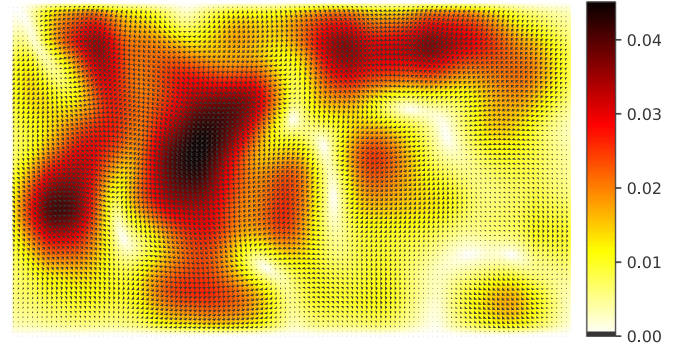
(b) $\zeta = 0.008$

FIG. 2. Magnitude of the velocity field for the straight channel ($W = L_y$) for different values of ζ at $\gamma = 0.04$ and $\varphi = 1.0$. The underlying colormap depicts the magnitude of the velocity field according to the color bar on the right. The black arrows describe the flow direction.

and wait for equilibration before recording data. We considered 100 realizations to improve the accuracy and minimize statistical errors. Unless otherwise stated, simulation parameters throughout this paper are $N = 400$, $\mu = 4.0$, $k = 0.4$, $k_w = 0.2$, $R = 8.0$, $\lambda = 3.0$, and $\xi = 1.0$. We tested that the presented results are robust against reasonable changes in these parameters.

III. RESULTS AND DISCUSSION

A. The role of the channel on rectification of cells

We first consider the case of the straight channel ($W = L_y$) where the entropic barrier disappears. At low activity (e.g., $\zeta = 0.001$), velocities are perpendicular to the boundary and symmetrically distributed near the boundary [Fig. 2(a)], and there is no flow. At a threshold value of the activity strength ζ which depends on γ and φ, the velocity field spontaneously transforms to a nonuniform and nonsymmetric distribution configuration that drives the flow. We note that the similar activity threshold also exists in the absence of confining walls [39,45]. When the activity strength (e.g., $\zeta = 0.008$) is larger than the activity threshold, the system is unstable to bend instabilities, and the streamlines become oscillatory; thus active turbulence appears [Fig. 2(b)]. Therefore, the microscopic dipolar interaction between cells based on their deformations drives the system out of equilibrium. The similar active
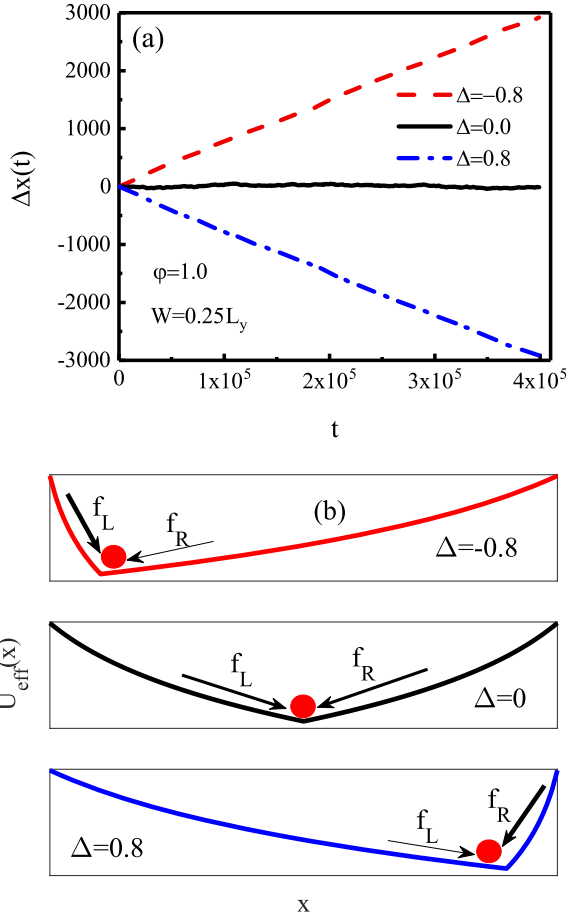
FIG. 3. (a) The average displacement $\Delta X(t)$ of cells as a function of t for different Δ at $\varphi = 1.0$, $\gamma = 0.04$, $\zeta = 0.008$, and $W = 0.25L_y$. The tissue on average moves to the left for $\Delta < 0$ and to the right for $\Delta > 0$. There is no directional motion in a symmetrical structure ($\Delta = 0.0$). (b) The profiles of the effective entropic potential $U_{\text{eff}}(x)$ for different Δ. In one period, the left side of the potential is steep for $\Delta < 0$, and the right side is steep for $\Delta > 0$. f_L and f_R are the amplitudes of the average forces from the left and right side of the potential, respectively.

FIG. 4. The average velocity V_x as a function of the minimum width W/L_y of the channel. (a) For different values of (γ, ζ) at $\varphi = 1.0$. (b) For different values of φ at $\gamma = 0.04$ and $\zeta = 0.008$.

turbulence also appears in confined active nematics [45]. How to control and harness this active turbulence is an interesting and important problem. To overcome this problem, we will focus our investigations on how to rectify active turbulence into directional motion by using the asymmetric channel.

For the convenience of discussion, we use the effective entropic potential obtained through the elimination of the y coordinate by assuming the equilibrium in the orthogonal direction [46]. The effective entropic potential is defined as $U_{\text{eff}}(x) \propto -k_B T \ln[2h(x)/R]$, where $2h(x)$ is the width of the channel, k_B is the Boltzmann constant, and T is the absolute temperature. Although this effective entropic potential is only a rough estimate, it is helpful for us to analyze the rectification mechanism of cells. The profiles of $U_{\text{eff}}(x)$ for different Δ are shown in Fig. 3(b). We next will explore how the properties (the asymmetry Δ and the minimum width W) of the channel affect the directional motion of cells in Figs. 3 and 4.

Figure 3(a) shows the average displacement $\Delta X(t)$ of cells vs t for different Δ at $\gamma = 0.04$ and $\zeta = 0.008$. In this case,
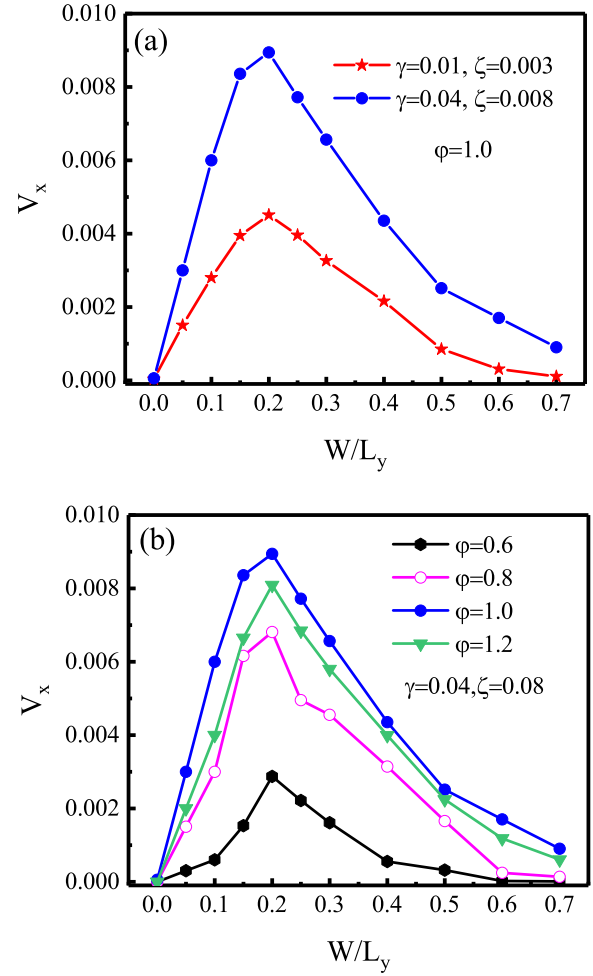
the system is unstable to bend instabilities, and the streamlines become oscillatory [see the velocity field shown in Fig. 7(b) below at $\Delta = -0.8$ and $W = 0.25L_y$], which shows that the local active forces proportional to the deformation of cells are able to drive the system out of equilibrium. It is found that cells on average move to the right for $\Delta < 0$ (e.g., $\Delta = -0.8$) and to the left for $\Delta > 0$ (e.g., $\Delta = 0.8$). The directed transport disappears at $\Delta = 0$. The direction of the macroscopic motion is determined by the asymmetry of the channel. A qualitative explanation of this behavior is presented as follows. In order to analyze the movement direction of cells, we use the force from the effective entropic potential [$f_x = -\partial U_{\text{eff}}(x)/\partial x$] and define f_L and f_R as the amplitudes of the average forces from the left and right side of the potential, respectively. The force from the effective entropic potential always drives cells to the minima of the potential. The greater the amplitude (f_L or f_R) of the force, the harder it is for cells to pass across the entropic barrier. Therefore, the movement direction of cells is determined by the competition between f_L and f_R. When $\Delta < 0$, the left side from the minima of the potential is steeper [shown in the top panel of Fig. 3(b)], $f_L > f_R$, and it is easier for cells to leave the potential valley

from the right; thus cells on average move to the right. When $\Delta = 0$, the effective entropic potential $U_{\text{eff}}(x)$ is symmetric [shown in the middle panel of Fig. 3(b)], cells feel the same force from the left and the right ($f_L = f_R$), and cells move to the left and the right with the same probability; thus directed transport disappears. In the same way, for $\Delta > 0$, the right side from the minima of the potential is steeper [shown in the bottom panel of Fig. 3(b)], $f_L < f_R$, so cells prefer to leave the potential valley from the left. Therefore, the direction of the transport is completely determined by the asymmetry of the channel. Because of the nematic nature of the interactions, macroscopic directional motion here is due to the ratchet effect, which is different from the directed motion induced by the spontaneous symmetry breaking (e.g., the flocking in active system with polar interactions). Since cells on average move in the opposite direction for Δ and $-\Delta$, we consider only the case of $\Delta < 0.0$ in the following.

How the minimum width W/L_y of the channel affects the average velocity V_x is shown in Figs. 4(a) and 4(b) for different cases. It is found that V_x is a peaked function of W/L_y. This can be explained as follows. When the channel is too narrow ($W/L_y \to 0$), the channel is almost closed and cells cannot pass cross the bottleneck of the channel; thus V_x tends to zero. When $W/L_y \to 1$, the channel becomes almost straight, and the asymmetry of the channel becomes negligible; thus the ratchet effect disappears and V_x converges to zero. Too wide or too narrow channels will weaken the rectification of cells. Therefore, there exists an optimal value of W/L_y at which V_x takes its maximal value. Note that the optimal minimum width of the channel is about $W/L_y = 0.2$, and this value hardly changes when the system parameters are varied.

B. The role of the nonequilibrium driving on rectification of cells

In this section we set $\Delta = -0.8$ and explore the directed transport of cells by varying the packing fraction φ, the active strength ζ, and the elasticity γ. We focus our investigations on how the activity from deformation of cells affects macroscopic directional motion. Note that the activity-driven system out of equilibrium is an effect of the cellular interactions alone; this effect will disappear for single, isolated cells at nonvanishing activity strength. Large activity strength does not necessarily produce large nonequilibrim driving. For example, even if ζ is large, but φ is small or the elasticity γ is large, the nonequilibrim driving is very small. Therefore, the nonequilibrium driving from deformation is determined by the competition among ζ, φ, and γ.

The dependence of the average velocity V_x on the packing fraction φ is shown in Figs. 5(a) and 5(b) for different cases. We find that the average velocity is a peaked function of the packing fraction. The activity driving the system out of equilibrium is significant for large φ and negligible for small φ. For $\varphi < \varphi_c$ (depending on ζ and γ), the nonequilibrium driving is negligible, and as a result the ratchet effect disappears. An increase of the packing fraction can have two results: (1) enhancing the nonequilibrim driving which facilitates the directed motion of cells or (2) increasing the difficulty of cells passing through the channel, which blocks the ratchet transport. For small φ (e.g., $\varphi = 0.3$), the direct contact between cells is negligible, and the activity from deformation
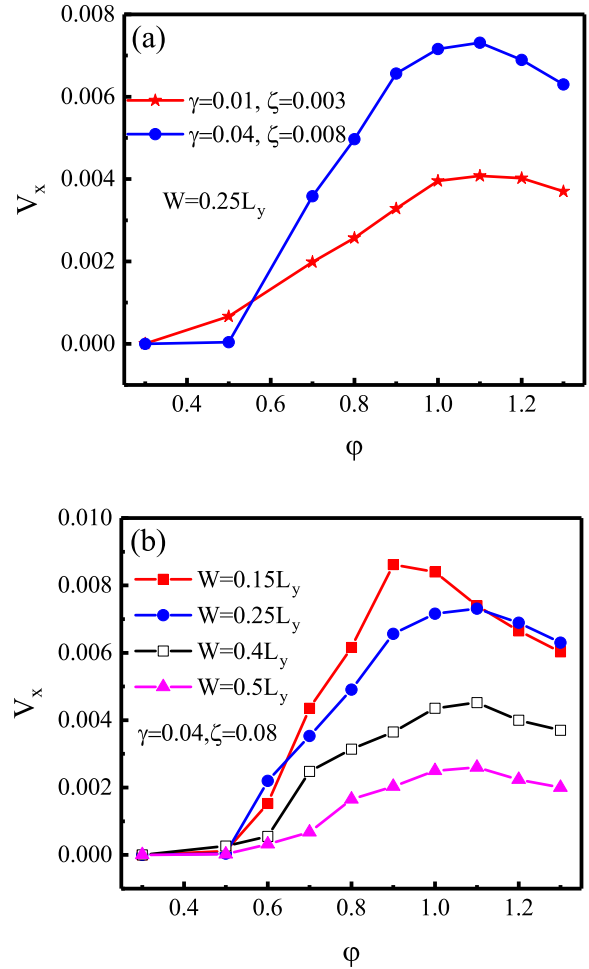

FIG. 5. Dependence of the average velocity V_x on the packing fraction φ. (a) For different values of (γ, ζ) at $W = 0.25L_y$. (b) For different values of W at $\gamma = 0.04$ and $\zeta = 0.008$.

almost disappears; thus V_x tends to zero. When the packing fraction increases from 0.3, the factor (1) first dominates the transport, thus V_x increases with φ. However, when the packing fraction becomes large (e.g., $\varphi = 1.2$), the factor (2) dominates the transport; thus V_x decreases with increasing φ. Therefore, there exists an optimal value of φ (near $\varphi = 1.0$) at which the average velocity takes its maximal value. In addition, we can find from Fig. 5(b) that the position of the peak in the curves shifts slightly to large φ with the increase of W.

Figure 6 describes the average velocity V_x as a function of the active strength ζ for different γ at $\varphi = 1.0$. It is found that large ζ does not always promote rectification of cells, and there exists an optimal ζ (the peak in the curve) at which V_x takes its maxima value. The emergence of the peak in each curve can be explained as follows. When $\zeta \to 0$, the system is in equilibrium, and no macroscopic directional motion appears; thus V_x tends to zero. There exists a finite threshold ζ_c (depending on φ and γ) below which the activity is not enough to drive the system out of equilibrium, therefore the transport disappears. The finite threshold ζ_c appears because cells need to push (pull) strongly enough to cause sufficient deformation of their neighbors. From the velocity field shown
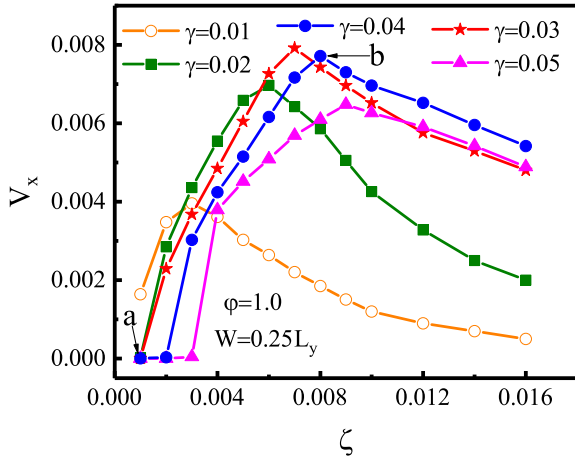
FIG. 6. Dependence of the average velocity V_x on the active strength ζ for different values of γ at $\varphi = 1.0$ and $W = 0.25L_y$.

FIG. 8. Phase diagram of the average velocity in the $\zeta - \gamma$ representation at $\varphi = 1.0$ and $W = 0.25L_y$. The average velocity is maximal in region A and tends to zero in region B. The background represents the value of V_x according to the color bar on the right. The red dashed line represents the position of the peak in the V_x-ζ curve of for different γ.

in Fig. 7(a), when $\zeta < \zeta_c$ (e.g., $\zeta = 0.001$), velocities are perpendicular to the boundary and symmetrically distributed near the boundary, and the system is in equilibrium. Note that ζ_c increases with the increase of γ and decreases with the increase of φ. When $\zeta > \zeta_c$, the active force is able to drive the system out of equilibrium [see the velocity field shown in Fig. 7(b)], and cells can pass across the entropic barrier [shown in the top panel of Fig. 3(b)]; thus the ratchet transport occurs. However, at high activities (e.g., $\zeta > 0.01$), the system is more out of equilibrium, and the active force dominates the transport. If the active force is much greater than the force from the effective entropic potential (f_L or f_R), cells
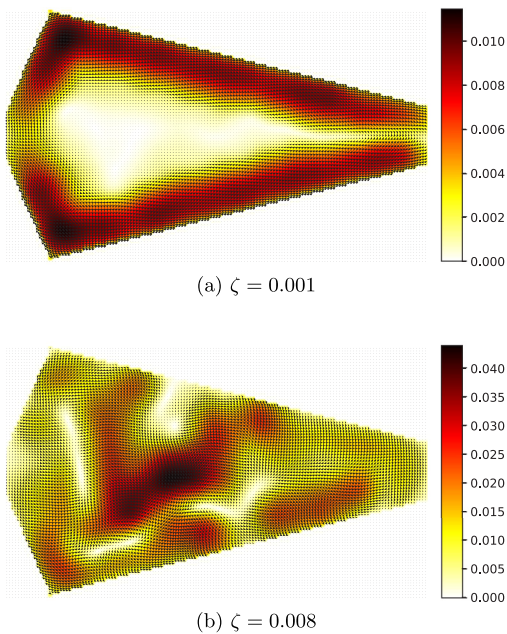
can easily pass across the entropic barrier, and the entropic barrier becomes less important. In this case, the movement direction of cells is determined by not only the asymmetry of the channel but also the active force. When the active force determines the direction of movement, cells move in different directions due to the random direction of the active force; thus the directed velocity on average is small. Although a single cell moves very fast, the rectification of the system becomes weak. In the extreme case of infinite active force, cells can hardly feel the existence of the entropic barrier, the movement direction of cells is completely determined by the active force, and cells move to the left and the right with the same probability; thus the ratchet effect disappears. Therefore, there exists an optimal ζ at which the average velocity takes its maximal value.

From Fig. 6 we also find that the position of the peak in the curves shifts to large ζ with an increase in γ. This can be explained as follows. The peak corresponds to the best match between the nonequilibrium driving and the entropic barrier. For a fixed entropic barrier, the optimal nonequilibrium driving must be required to obtain the best rectification. The optimal nonequilibrium driving depends on the competition between the active strength ζ and the elasticity γ. The nonequilibrium driving increases with the increase of ζ and decreases with the increase of γ. Therefore, the higher γ value, the more activity ζ is required to obtain the optimal nonequilibrium driving; thus the position of the peak shifts to large ζ with an increase in γ.

To study in more detail the dependence of the average velocity V_x on the active strength ζ and the elasticity γ, we plotted the phase diagram of the average velocity in the ζ-γ representation at $\varphi = 1.0$ in Fig. 8. The red dashed line describes the position of the peak the V_x-ζ curve shown in Fig. 6 for different γ. When γ gradually increases, the position of the peak shifts to large ζ. The color of the background indicates that when γ continuously increases from 0.01, the

(a) $\zeta = 0.001$

(b) $\zeta = 0.008$

FIG. 7. Magnitude of the velocity field for different values of ζ at $\gamma = 0.04$, $\varphi = 1.0$, and $W = 0.25L_y$, corresponding the points a and b in Fig. 6. The underlying colormap depicts the magnitude of the velocity field according to the color bar on the right. The black arrows describe the flow direction.
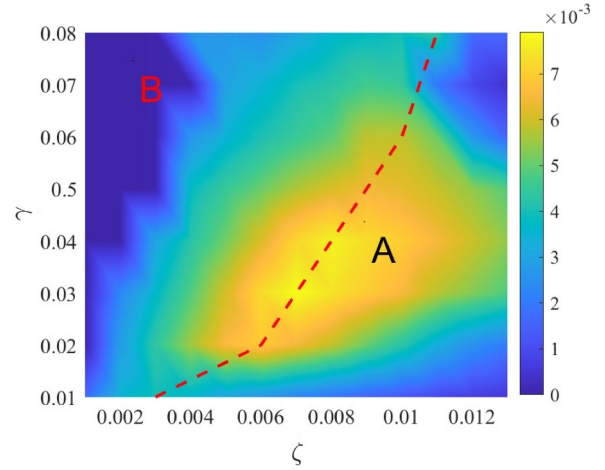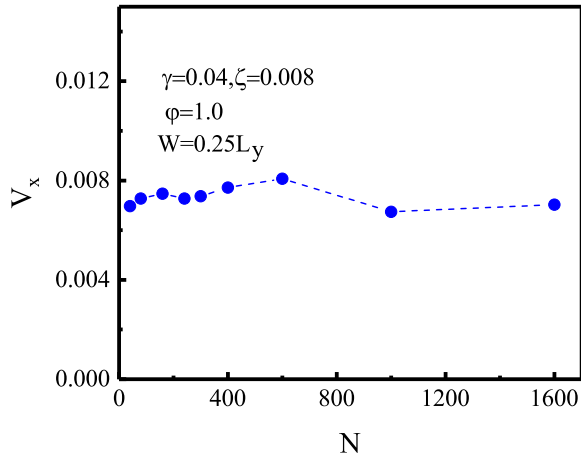
FIG. 9. The average velocity V_x as a function of the total cell number N at $\gamma = 0.04$, $\zeta = 0.008$, $\varphi = 1.0$, and $W = 0.25L_y$. The average velocity is obtained irrespective of the system size.

height of the peak first increases, reaches the highest, and then decreases. V_x is a peaked function of γ at a given ζ. Therefore, there exists an optimized parameter region (region A) of (ζ, γ) where V_x takes its maximal value. In this region, the nonequilibrium driving (depending on ζ and γ) perfectly matches the entrpoic barrier, which facilitates the rectification of cells. However, in region B, the nonequilibrium driving is either very large or very small, which does not match the entropic barrier; thus V_x is very small. Note that this phase diagram does not change qualitatively when the other parameters are varied.

In Fig. 9 we investigate the effect of the system size on rectification of cells, the average velocity V_x vs the total cell number N. Here we fix $R = 8.0$, $\varphi = 1.0$, and $W = 0.25L_y$, and the system size (L_x and L_y) changes correspondingly with the total cell number N. It is found that no significant change in the average velocity V_x when the system size N changes, which shows that the rectification of cells is independent of the system size. Therefore, our results are universal rather than finite-size effects.

Finally, we briefly discuss the effect of the spontaneous symmetry breaking on rectification of cells. If the polar alignment interaction between cells is considered, the spontaneous symmetry breaking will occur, and cells will move in the same direction together. The directed transport of cells is determined by the competition between the ratchet effect and the spontaneous symmetry breaking. When the polar alignment interaction is small, the ratchet effect dominates the transport. In this case, the polar alignment interaction causes cells to move together, which facilitates the rectification of cells. When the polar alignment interaction is very large, the spontaneous symmetry breaking dominates the transport, and the asymmetry of the channel (the ratchet effect) can be negligible. In this case, all cells move in the same direction,

but the direction is random, independent of the asymmetry of the channel; thus the ratchet effect disappears.

IV. CONCLUSION AND OUTLOOK

In summary, we studied the directed transport of deformable active cells in the asymmetric periodic channel using the phase-field model. We show that the microscopic dipolar interaction between cells based on their deformations can drive the system out of equilibrium and induce macroscopic directional motion in the periodic asymmetric channel. The asymmetry of the channel completely determines the direction of the macroscopic motion. The average velocity is positive for $\Delta < 0$, negative for $\Delta > 0$, and zero at $\Delta = 0.0$. This indicates that collective turbulent-like motion, driven by the local active forces proportional to the deformation of cells, can be controlled and utilized. The nonequilibrium driving from deformation is determined by the competition among the active strength, the elasticity, and the packing fraction. There exists an optimized nonequilibrium driving at which the average velocity takes its maximal value. The optimized minimum width of the channel can facilitate macroscopic directional motion of cells.

The macroscopic directional motion in our work is due to the ratchet effect (cells on average moving in a given direction), and the direction of motion can be controlled, which is different from in previous works [12–19] where macroscopic directional motion is caused by the spontaneous symmetry breaking (all cells moving in the same direction), but the direction of motion is random. Our findings are relevant to understanding how macroscopic directional motion relates to the local force transmission mediated by cell-cell contacts in cellular monolayers. Using the local (microscopic) active driving, the motion direction of cells can be easily controlled by adjusting the structure of the channel. We expect these results to trigger further experimental studies of collective motion in cellular monolayers, for example, Madin-Darby canine kidney or human breast cancer cells [47], where a bootstrap feedback between shape deformations and intercellular driving allows cells of isotropic shape. It is hoped that macroscopic directional motion can be observed in these experiments through the special geometric constraints.

[1] N. V. Jordan, G. L. Johnson, and A. N. Abell, Cell Cycle **10**, 2865 (2011).

[2] E. H. Barriga, K. Franze, G. Charras, and R. Mayor, Nature (London) **554**, 523 (2018).

[3] P. Friedl, J. Locker, E. Sahai, and J. E. Segall, Nat. Cell Biol. **14**, 777 (2012).

[4] A. Brugues, E. Anon, V. Conte, J. H. Veldhuis, M. Gupta, J. Colombelli, J. J. Munoz, G. W. Brodland, B. Ladoux, and X. Trepat, Nat. Phys. **10**, 683 (2014).

[5] K. Chiou and E. M. S. Collins, Dev. Biol. **433**, 155 (2018).

[6] E. Putzig and A. Baskaran, Phys. Rev. E **90**, 042304 (2014).

[7] A. Cavagna, I. Giardina, T. S. Grigera, A. Jelic, D. Levine, S. Ramaswamy, and M. Viale, Phys. Rev. Lett. **114**, 218101 (2015).

[8] L. Giomi, M. J. Bowick, X. Ma, and M. C. Marchetti, Phys. Rev. Lett. **110**, 228101 (2013).

[9] H. H. Wensink, J. Dunkel, S. Heidenreich, K. Drescher, R. E. Goldstein, H. Lowen, and J. M. Yeomans, Proc. Natl. Acad. Sci. USA **109**, 14308 (2012).

[10] R. Voituriez, J. F. Joanny, and J. Prost, Europhys. Lett. **70**, 404 (2005).

[11] C. Blanch-Mercader, V. Yashunsky, S. Garcia, G. Duclos, L. Giomi, and P. Silberzan, Phys. Rev. Lett. **120**, 208101 (2018).

[12] G. Duclos, C. Blanch-Mercader, V. Yashunsky, G. Salbreux, J.-F. Joanny, J. Prost, and P. Silberzan, Nat. Phys. **14**, 728 (2018).

[13] T. N. Shendruk, A. Doostmohammadi, K. Thijssen, and J. M. Yeomans, Soft Matter **13**, 3853 (2017).

[14] S. Chandragiri, A. Doostmohammadi, J. M. Yeomans, and S. P. Thampi, Phys. Rev. Lett. **125**, 148002 (2020).

[15] A. Bricard, J.-B. Caussin, N. Desreumaux, O. Dauchot, and D. Bartolo, Nature (London) **503**, 95 (2013).

[16] K.-T. Wu, J. B. Hishamunda, D. T. Chen, S. J. DeCamp, Y.-W. Chang, A. Fernandez-Nieves, S. Fraden, and Z. Dogic, Science **355**, eaal1979 (2017).

[17] T. Sanchez, D. T. Chen, S. J. DeCamp, M. Heymann, and Z. Dogic, Nature (London) **491**, 431 (2012).

[18] K. Suzuki, M. Miyazaki, J. Takagi, T. Itabashi, and S. Ishiwata, Proc. Natl. Acad. Sci. USA **114**, 2922 (2017).

[19] V. Yashunsky, D. J. G. Pearce, C. Blanch-Mercader, F. Ascione, P. Silberzan, and L. Giomi, Phys. Rev. X **12**, 041017 (2022).

[20] R. Mueller, J. M. Yeomans, and A. Doostmohammadi, Phys. Rev. Lett. **122**, 048004 (2019).

[21] R. Mueller and A. Doostmohammadi, arXiv:2102.05557.

[22] P. Hänggi and F. Marchesoni, Rev. Mod. Phys. **81**, 387 (2009).

[23] C. J. O. Reichhardt and C. Reichhardt, Annu. Rev. Condens. Matter Phys. **8**, 51 (2017).

[24] P. K. Ghosh, V. R. Misko, F. Marchesoni, and F. Nori, Phys. Rev. Lett. **110**, 268301 (2013).

[25] Y. Li, P. K. Ghosh, F. Marchesoni, and B. Li, Phys. Rev. E **90**, 062301 (2014).

[26] P. K. Ghosh, P. Hänggi, F. Marchesoni, and F. Nori, Phys. Rev. E **89**, 062115 (2014).

[27] Y. F. He, B. Q. Ai, C. X. Dai, C. Song, R. Q. Wang, W. T. Sun, F. C. Liu, and Y. Feng, Phys. Rev. Lett. **124**, 075001 (2020).

[28] B. Q. Ai, Q. Y. Chen, Y. F. He, F. G. Li, and W. R. Zhong, Phys. Rev. E **88**, 062129 (2013).

[29] X. Hong, K. W. Desmond, D. Chen, and E. R. Weeks, Phys. Rev. E **105**, 014603 (2022).

[30] M. B. Wan, C. J. Olson Reichhardt, Z. Nussinov, and C. Reichhardt, Phys. Rev. Lett. **101**, 018102 (2008).

[31] C. Grossert, M. Leder, S. Denisov, P. Hänggi, and M. Weitz, Nat. Commun. **7**, 10440 (2016).

[32] Z. Zheng, G. Hu, and B. Hu, Phys. Rev. Lett. **86**, 2273 (2001).

[33] A. Kaiser, A. Peshkov, A. Sokolov, B. ten Hagen, H. Löwen, and I. S. Aranson, Phys. Rev. Lett. **112**, 158101 (2014).

[34] C. Reichhardt and C. J. Olson Reichhardt, Phys. Rev. E **88**, 062310 (2013).

[35] J. C. Bellizotti Souza, N. P. Vizarim, C. J. O. Reichhardt, C. Reichhardt, and P. A. Venegas, New J. Phys. **24**, 103030 (2022).

[36] J. Katuri, D. Caballero, R. Voituriez, J. Samitier, and S. Sanchez, ACS Nano **12**, 7282 (2018).

[37] N. Nikola, A. P. Solon, Y. Kafri, M. Kardar, J. Tailleur, and R. Voituriez, Phys. Rev. Lett. **117**, 098001 (2016).

[38] R. Alert and X. Trepat, Annu. Rev. Condens. Matter Phys. **11**, 77 (2020).

[39] G. Zhang, R. Mueller, A. Doostmohammadi, and J. M. Yeomans, J. R. Soc. Interface **17**, 20200312 (2020).

[40] G. Peyret, R. Muller, J. d'Alessandro, S. Begnaud, P. Marcq, R. M. Mege, J. M. Yeomans, A. Doostmohammadi, and B. Ladoux, Biophys. J. **117**, 464 (2019).

[41] M. Foglino, A. N. Morozov, O. Henrich, and D. Marenduzzo, Phys. Rev. Lett. **119**, 208002 (2017).

[42] D. Wenzel and A. Voigt, Phys. Rev. E **104**, 054410 (2021).

[43] B. Loewe, M. Chiang, D. Marenduzzo, and M. C. Marchetti, Phys. Rev. Lett. **125**, 038003 (2020).

[44] J. W. Cahn and J. E. Hilliard, J. Chem. Phys. **28**, 258 (1958).

[45] A. Doostmohammadi and J. M. Yeomans, Eur. Phys. J. Spec. Top. **227**, 2401 (2019).

[46] D. Reguera and J. M. Rubi, Phys. Rev. E **64**, 061106 (2001).

[47] T. B. Saw, A. Doostmohammadi, V. Nier, L. Kocgozlu, S. Thampi, Y. Toyama, P. Marcq, C. T. Lim, J. M. Yeomans, and B. Ladoux, Nature (London) **544**, 212 (2017).